Gas Concentration Measurement by Coherent Raman Anti-Stokes Scattering

P. R. RÉGNIER,* F. MOYA,* AND J. P. E. TARAN†
Office National d'Etudes et de Recherches Aérospatiales (ONERA), Châtillon, France

A novel method for gas concentration measurement is described. This method is based on a four wave mixing process: two collinear light beams of frequencies ω_1 and ω_2 generate a collinear (anti-Stokes) wave at frequency $2\omega_1 - \omega_2$ when traversing a gas containing a Raman active molecular species with vibrational frequency $\omega_v = \omega_1 - \omega_2$. The intensity of the new wave is proportional to the square of the number density of resonant molecules. This scattering is much more intense than spontaneous Raman scattering. Possible experimental set-ups are reviewed. Typical results obtained with H_2 gas are also presented: the concentration in a hydrocarbon flame was mapped, and small jets through the atmosphere were photographed in anti-Stokes light. The limitations of the method are discussed, and its field of application is assessed.

1. Introduction

SPONTANEOUS Raman scattering is a very attractive tool for point gas concentration measurements in aerodynamic flows.[1-6] In particular, it does not perturb the flow and does not interfere with any chemical reaction that could take place within. Furthermore, its sensitivity is sufficient for the probing of gas mixtures with pressures ranging from a few atmospheres down to a few torrs.[1] To this end, one generally makes use of pulsed ruby[1] or N_2 lasers[2,5] for the illumination of the gas, and monochromators[1-6] or interference filters for the separation of the Raman lines; cw argon-ion lasers are also used by a number of workers.[3,4,6] Detection is often achieved with gated photomultipliers and pulse counting electronics.

Similar equipment is required for the remote detection of atmospheric pollutants.[7,8] Detectivities approaching a few ppm at ranges up to 1 km have recently been obtained.[8,9]

Both types of measurements require low ambient light levels and drastic rejection of the pump laser radiation. In particular, night-time operation is preferable,[7] although this may be not necessary for short wavelength excitation.[8]

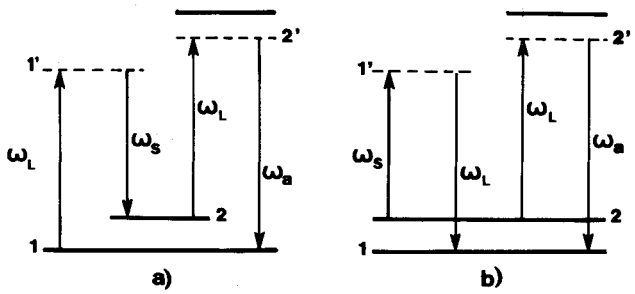

Fig. 1 Coherent Raman anti-Stokes scattering. Level 1 is the ground state; level 2 is any Raman active level (in the experiments described, 2 is a vibrational level). The scattering process is instantaneous. Resonance enhancement can take place if either of the virtual levels 1′ and 2′ is close to an absorption.

Received June 27, 1973; presented as Paper 73-702 at the AIAA 6th Fluid and Plasma Dynamics Conference, Palm Springs, Calif., July 16–18, 1973; revision received December 10, 1973. The authors would like to thank Y. R. Shen for helpful comments.
Index categories: Lasers; Reactive Flows.
* Student Scientist.
† Research Scientist.

The purpose of this study was to investigate whether the process called "three wave mixing"[10] or "coherent Raman anti-Stokes scattering"[11] (CRAS) can lead to improved sensitivity and operational simplicity. Experimentally, CRAS is observed when intense collinear light beams at ω_1 and ω_2 are sent simultaneously into the gas sample to analyze. If some molecular species with a Raman active vibrational mode at frequency $\omega_v = \omega_1 - \omega_2$ is present, light is generated at $\omega_3 = 2\omega_1 - \omega_2$ with an intensity proportional to the square of the Raman nonlinear susceptibility of the gas mixture. The generation of this wave proceeds from two distinct mechanisms, as pointed out by Bloembergen[12]:

1) a parametric process is associated with the real part of the Raman susceptibility χ, two laser quanta at ω_1 scattering into a Stokes quantum at ω_2 and an anti-Stokes quantum at ω_3 (Fig. 1a), or vice versa depending on the relative phases of the waves;

2) a Raman process is associated with the imaginary part of χ; two simultaneous transitions between the same initial and the same final states are involved (Fig. 1b), resulting in an absorption at ω_2 and a generation at ω_3 or vice versa, also depending on the phases of the waves.

A number of authors have used this technique for the measurement of the nonresonant part of the Raman susceptibility in gases,[13,14] the study of anharmonic scattering in H_2[11] and the plotting of line profiles.[10,15] It is shown here that it can also be used for concentration measurements in gases, since the Raman susceptibility is proportional to the number density of the molecules.

The theory of the effect is well known and will only be briefly outlined; important parameters are: a) the linear dispersion of the medium; b) the vibrational frequency and line width of the Raman nonlinear susceptibility, which depend on foreign gases, pressure, and temperature; c) the pump beam intensities and geometries; and d) the occupation of the various energy levels of the molecules, with temperature measurement as a possible application.

Experimental investigations demonstrated the feasibility of detecting molecular gases with the now standard equipment[10,11,13-15] composed of a ruby laser and a stimulated Raman scattering (SRS) oscillator. Promising results could be obtained in the mapping of the distribution of H_2 in a natural gas flame. The difficult problems of the probing of flows between rotor blades on compressors, and of the analysis of combustions and explosions in very short times, will readily be solved by this technique. The remote sensing of pollution is also possible; however, the instrument is double-ended and the detectivity is inherently limited to 10–100 ppm (but the latter will improve with resonance excitation). Finally, we were also able to photo-

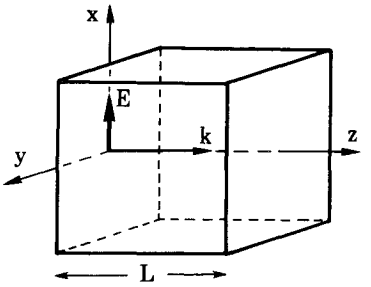

Fig. 2 Fields and wave vectors for the anti-Stokes generation in a gas sample.

graph a 1-mm-diam supersonic jet of H_2 in anti-Stokes light, which opens the field of flow and mixing layer visualization by direct photography.

2. Wave Interaction

2.1. Basic Equations

The problem of the generation of the anti-Stokes sidebands in the course of the stimulated Raman interaction has long ago been given careful attention; in particular, excellent presentations have been given by Bloembergen[12] and by Yariv.[16] The treatment followed here parallels the one given by Bloembergen.

Take two intense plane light waves of frequencies ω_1 and ω_2 (with $\omega_2 < \omega_1$), with parallel field vectors, and with parallel propagation vectors k_1 and k_2 aligned along the z axis in a Cartesian coordinate system (Fig. 2). Let these waves traverse a pure molecular gas located between plane boundaries at $z = 0$ and $z = L$; the gas will be assumed to possess an anharmonic Raman active, vibrational mode with $0 \to 1$ transition of frequency $\omega_v \simeq \omega_1 - \omega_2$, and to further present no absorption at frequencies ω_1, ω_2 and $\omega_3 = 2\omega_1 - \omega_2$, while the index of refraction will be taken as unity. Under the assumption of quasi-stationarity, one expands the electric fields in terms of their envelopes as

$$E_i = \tfrac{1}{2}[\mathscr{E}_i e^{i(k_i z - \omega_i t)} + \text{c.c.}]$$

One may then write the third-order nonlinear polarization in the gas at frequency ω_3 which results from the presence of fields E_1 and E_2

$$P_3(x,y,z) = \tfrac{1}{8}\chi(x,y,z)\mathscr{E}_1{}^2\mathscr{E}_2{}^* e^{i(k'z-\omega_3 t)} + \text{c.c.}$$

with $k' = 2k_1 - k_2$. Here, the appropriate component of the (third order) Raman susceptibility tensor χ is taken to be a function of position; one thus allows for the local inhomogeneities in pressure and temperature in the gas sample which would result from aerodynamic instabilities. Polarization P_3 is responsible for the generation of an electromagnetic wave E_3, with wave vector k_3 parallel with k_1 and k_2; the corresponding electric field envelope $\mathscr{E}_3$ can be written at the exit boundary:

$$\mathscr{E}_3(x,y,L) = -\frac{i\pi\omega_3}{2c}\mathscr{E}_1{}^2\mathscr{E}_2{}^* \times \int_0^L \chi(x,y,z)e^{i\Delta kz}dz \qquad (1)$$

where $\Delta k = k' - k_3$; the integration was carried out with the additional assumption that $\mathscr{E}_1$, $\mathscr{E}_2$ and χ are not perturbed by the interaction and that the diffraction of the anti-Stokes wave is negligible, which holds if

$$\frac{1}{|\chi|}\left|\frac{\partial\chi}{\partial x, \partial y}\right| \ll \left(\frac{k_3}{L}\right)^{1/2} \qquad (2)$$

The intensity distribution across the exit plane follows from

$$I_i = (c/8\pi)|\mathscr{E}_i|^2$$

yielding:

$$I_3(x,y,L) = \left(\frac{4\pi^2\omega_3}{c^2}\right)^2 I_1{}^2 I_2 \times \left|\int_0^L \chi(x,y,z)e^{i\Delta kz}dz\right|^2 \qquad (3)$$

One can see readily that Eq. (3) gives the integral of the susceptibility along lines of constant x and y, in terms of the distribution of intensity $I_3(x,y,L)$, and provided the phase factor Δkz is small.

The next step is to express χ in terms of the number density of the gas to be detected. For any gas, χ can be given the well known[12] expansion

$$\chi = \chi' + i\chi'' + \chi^{NR}$$

The real and imaginary parts χ' and χ'' of the resonant susceptibility arise from the motion of the nuclei.

The nonresonant susceptibility χ^{NR} is contributed by the electron cloud and the wings of remote resonances. It is real and independent of ω_1 and ω_2 if ω_1 and ω_2 are far from an electronic absorption; furthermore, it is proportional to the number density N of the molecules

$$\chi^{NR} = N\alpha^{NR}$$

On the other hand, the resonant part can be expressed in terms of the differential Raman scattering cross section per molecule $d\sigma/d\Omega$. A derivation similar to that of Shen and Bloembergen or Maier et al.[17] leads to the following formula, neglecting dispersion in the nonlinearity:

$$\chi' + i\chi'' = N\beta\Delta \frac{\omega_v}{\omega_v{}^2 - (\omega_1-\omega_2)^2 - i\gamma(\omega_1-\omega_2)} \qquad (4)$$

with γ damping constant, and $\beta = (2c^4/\hbar\omega_2{}^4)(d\sigma/d\Omega)$. The factory Δ, assumed constant by virtue of our stationarity condition on χ, is the difference in probability of finding the molecule in the ground and first vibrational states: $N\Delta$ is thus the population difference density between the two states. One has in general $\Delta = [1-\exp(-\hbar\omega_v/kT)]/Q$ where T is the temperature and Q the vibrational partition function $Q = [1-\exp(-\hbar\omega_v/kT)]^{-1}$. Introducing the detuning $\Delta\omega = \omega_v - (\omega_1 - \omega_2)$, and assuming $|\Delta\omega| \ll \omega_v$, Eq. (4) becomes

$$\chi' + i\chi'' = N\beta\Delta \frac{1}{2\Delta\omega - i\gamma} \qquad (4')$$

The terms χ' and $-\chi''$ as given by Eq. (4) satisfy the Kramers-Kronig relations.[12] Note also that χ'', imaginary part of the anti-Stokes susceptibility, corresponds to $-\chi''$ in Bloembergen's notation.[12]

With the exception of gases like H_2 whose Q lines do not overlap, Δ can be taken unity over the temperature range $0 < T < \hbar\omega_v/2k$ (for H_2, Δ is picked equal to the fractional occupation of the rotational level J corresponding to the particular $Q(J)$ line being probed, e.g., $\Delta = 0.67$ for $Q(1)$ at $T = 300°\text{K}$). One thus sees that over a large temperature domain, provided the Raman cross section $d\sigma/d\Omega$, the Raman linewidth γ and the detuning are known, Eq. (3) offers a means of measuring the number density N. The problem further simplifies if the excitation is done exactly on resonance ($\Delta\omega = 0$), or far off resonance ($|\Delta\omega| \gg \gamma$). The implications and merits of these two experimental situations will be discussed in Sec. 2.3.

We shall now review the properties of the main parameters in Eqs. (3) and (4).

2.2. Phase Mismatch

The exponential in Eq. (3) can be taken as unity provided $z < l_c$, where l_c is given by $\Delta k l_c = \pi$. The mismatch Δk for parallel propagation vectors is a function of the medium's dispersion and of the frequency difference $\omega_1 - \omega_2 \simeq \omega_v$. One has[14]

$$l_c = (\pi c/\omega_v{}^2)[2\,\partial n/\partial\omega + \omega_1\,\partial^2 n/\partial\omega^2]^{-1}$$

where n is the index of refraction. For air under standard temperature and pressure conditions, l_c is given in Table 1; one can see that l_c is in general comparable to or larger than the thickness of the samples or wind-tunnel flows one has to probe. However, l_c is inversely proportional to the number density, and care must be taken with high pressure gases.

2.3. Spectral Properties of χ—Detection of Gases in Mixtures

Far from an electronic absorption, χ does not depend strongly on laser frequency, thus one has not the same advantage going to shorter wavelengths one had with spontaneous Raman scattering (with the ω^4 dependance of the scattering cross section). But in the vicinity of an electronic absorption χ may

Table 1 Frequency shifts of some gases, with corresponding spontaneous Raman scattering cross sections and coherence lengths for four wave mixing in air

gas	ω_v(cm^{-1})	$\left(\frac{d\sigma}{d\Omega}\right)_{gas}/\left(\frac{d\sigma}{d\Omega}\right)_{N_2}$ [a]	l_c(cm)
O_3	1103	4.0	325
SO_2	1151	5.5	260
N_2O	1287	2.7	210
CO_2	1286	1.0	210
	1388	1.5	180
O_2	1556	1.2	140
NO	1877	0.55	98
CO	2143	1.2	75
N_2	2331	1.0	63
H_2S	2611	6.6	51
CH_4	2914	8.0	38.5
	3020	0.79	38
H_2O	3652		26
H_2 [Q(1)]	4155	2.2	20
	$(d\sigma/d\Omega)_{N_2} = (4.4 \pm 1.7) \times 10^{-31}$ cm^2/sr		

[a] After Chang and Fouche.[9]

increase by several orders of magnitude, with a resultant increase in I_3.

The variations of χ vs detuning as given by Eq. (4) are plotted in Fig. 3. The profile of χ'' is similar to that of the spontaneous Raman line, whereas χ' has a $\Delta\omega^{-1}$ dependance in the vicinity of the center frequency. Note also that for $\omega_1 - \omega_2 \simeq 0$, one has $\chi' \simeq N\beta/\omega_v$, which is in general on the same order of magnitude as χ^{NR} in a pure gas; on the other side of the line, one has $\chi' \simeq N\beta\omega_v/(\omega_1-\omega_2)^2$, which decays more rapidly. The real components of the susceptibility, namely χ^{NR} which extends over the whole spectral range, and χ' which decays slower than the spontaneous Raman line away from resonance, may render the detection of a constituent in a mixture less selective than spontaneous Raman scattering, due to line overlap.

Assume that a gas characterized by its Raman parameters χ_1, β_1, ω_{v_1}, and γ_1, and its number density N_1 is to be detected in a buffer gas (number density N_0) with nonresonant susceptibility $\chi_0{}^{NR} = N_0\alpha_0{}^{NR}$. This can be done best on resonance ($\Delta\omega = 0$), and provided one has $\chi_1'' > \chi_0{}^{NR}$; hence the condition $N_1 \geqq N_1{}^0$ with

$$N_1{}^0 = (\gamma_1 \alpha_0{}^{NR}/\beta_1)N_0 \tag{5}$$

One should point out that:

a) $N_1{}^0/N_0$ is the minimum concentration that can be detected in a mixture. $N_1{}^0$ is not the minimum mensurable number density (e.g., for a pure gas), which depends only on the available laser and Stokes powers and the sensitivity of the anti-Stokes detecting equipment (see next section);

b) for simple molecules, $d\sigma/d\Omega$ and α^{NR} vary little with gas species.[9,14] The ratio $N_1{}^0/N_0$ therefore depends primarily on the linewidth γ_1;

c) one can give a crude estimate of $N_1{}^0/N_0$. For H_2, taking $d\sigma_1/d\Omega = 10^{-30}$ cm^2/sr and $\gamma_1/2\pi c = 3 \times 10^{-2}$ cm^{-1} (Refs. 18 and 19), one gets $N_1{}^0/N_0 \simeq 10^{-5}$ assuming the buffer gas causes no line broadening. For other gases, the Raman frequencies and cross sections are well known; but little experimental data has been published so far on their linewidths, with the exception of N_2 (Ref. 18). In general, the Q transitions constitute one broad line, the width of which is determined by the variation of the rotational constant B with vibrational quantum number and by the temperature; these widths range from 10^{-1} to 1 cm^{-1}, resulting in $N_1{}^0/N_0 = 10^{-5}$ to 10^{-4}.

The advantage of tuning the excitation exactly on resonance is obvious for the detection of weak concentrations. Unfortunately, both ω_v and γ depend to a limited extent on temperature, pressure, and buffer gas. For experimental situations where these variations are encountered, one may prefer to detune the excitation as was suggested in Ref. 14. For $|\Delta\omega| > \gamma$, the response of the medium is independent of γ and of the small shifts of ω_v, which are generally comparable to γ. The measurement then depends only on the detuning, which can be set or determined quite accurately; but one suffers a loss in the detectivity.

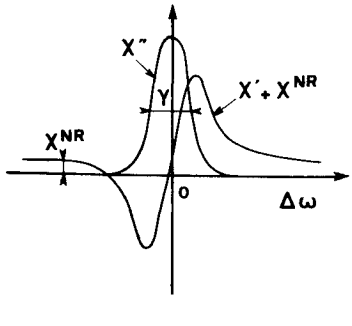

Fig. 3 Profile of the anti-Stokes Raman susceptibility for a pure gas in the vicinity of a vibrational line. χ^{NR} is not to scale, being 4 to 5 orders of magnitude smaller than χ'' at $\Delta\omega = 0$.

2.4. Beam Geometries and Intensities

Two classes of problems are encountered experimentally, namely visualization of a gas distribution across a whole aerodynamic field such as in a wind tunnel (in a fashion similar to interferometric or Schlieren methods), and point gas concentration measurements.

Visualization

For the first type of application, parallel beams are to be used, both for the laser and Stokes radiations. Equation (3) then applies. Crude estimates can be calculated for the anti-Stokes intensity obtained; for laser and Stokes beam intensities on the order of 1 Mw/cm^2 traversing a 1 cm thick sample of 10% H_2 in ambient air, $I_3 = 1$ Mw/cm^2. This is sufficient for exposing a high-speed photographic plate in 20 nsec. Should the sample contain only 0.1% of H_2, the same I_3 would be maintained with a 100 Mw/cm^2 laser beam and a 1 Mw/cm^2 Stokes beam. These figures indicate how the system scales with power. Some improvements in the sensitivity could also be obtained with an image intensifier.

Point measurements

For point gas concentration measurements, the collinear pump beams are focused into the sample through the same lens. The power collected is generated from the diffraction limited focal volume (the other regions before and after the focus giving negligible contributions), and in the same solid angle as the pump beams. This power is crudely independent of f-number[10]

$$P_3 \simeq \left(\frac{2}{\lambda}\right)^2 \left(\frac{4\pi^2\omega_3}{c^2}\right)^2 \chi^2 P_1{}^2 P_2 \tag{6}$$

where $\lambda = 2\pi c/\omega$ (with $\omega \simeq \omega_1 \simeq \omega_2 \simeq \omega_3$), and where P_1 and P_2 are the laser and Stokes powers, respectively. The focal volume is a cylinder with diameter $\phi = 4\lambda f/\pi d$ (where f is the focal length and d the common gaussian beam waist in the plane of the lens) and length $l = \pi\phi^2/2\lambda$ (we assume $l < l_c$).

More accurate calculations were done; a derivation similar to that of Ward and New[20] gives a formula which can be integrated numerically.[21] We found that 75% of the anti-Stokes power was generated from a volume of length 6 l. This was verified experimentally.[21] The study also showed that P_3 diminishes when f increases (a factor of 3 is found from $f = 3$ cm to $f = 50$ cm).

Crude estimates can be made for a typical case. Assume $P_1 = P_2 = 10$ kw, $f = 10$ cm, $d = 6$ mm; with a sample containing 100 ppm of H_2 in air, one obtains 1 μw of anti-Stokes power, scattered from a volume which does not exceed 20 μm in diameter and 500 μm in length. Spontaneous Raman scattering from the same focal volume with $P_1 = 10$ kw would yield only 10^{-12} w/sr in the Stokes sideband.

Focusing yields the largest anti-Stokes signal for given laser and Stokes powers. We can estimate the ultimate number density which can be measured for a gas, whether pure or to a dilution not exceeding that given by Eq. (5). Assuming a single anti-Stokes

photon is generated in a 20 nsec period, with $P_1 = P_2 = 1$ Mw, we get $N = 10^{10}$ cm^{-3} for H_2, corresponding to a partial pressure of 10^{-9} atm (10^{-8} atm for other gases, with larger γ). Experimentally P_1 and P_2 could be raised by 1 to 3 orders of magnitude, permitting further gains in detectivity.

2.5. Vibrational Population—Temperature Measurement

Equation (3) holds provided the interaction does not perturb the vibrational population. Therefore Δ must remain constant so that the measurements are meaningful; its equation, as given by Maier et al.,[17] is transcribed in our notation:

$$\frac{\partial \Delta}{\partial t} = -\beta\left(\frac{4\pi}{c}\right)^2 I_1 I_2 \frac{\gamma}{4\Delta\omega^2+\gamma^2}\Delta \qquad (7)$$

Take $\Delta(t=0) = 1$, $d\sigma/d\Omega = 10^{-30}$ cm^2/sr, $\Delta\omega = 0$, $\gamma/2\pi c = 1$ cm^{-1}, $\omega_2/2\pi c = 10^4$ cm^{-1}; assume further $I_1 = I_2 = 1$ Gw/cm^2 (such intensities are obtained at the focus of a lens with $f = 10$ cm for a 10 kw, $d = 3$ mm, beam). The initial slump rate of Δ is $|\partial\Delta/\partial t| \simeq 10^7$ sec^{-1}. An appreciable vibrational population of the $v = 1$ level is thus built up in a few nanoseconds: this property has been used for the investigation of vibrational relaxation in gases.[22]

It is therefore clear that care should be taken with point density measurements. Note also that an additional constraint is imposed if N is large ($N > 10^{19}$ cm^{-3}) due to SRS gain of the Stokes wave.[10] The condition that the Stokes wave passing through the focus undergoes less than 10% growth is given by $2gP_1/\lambda < 0.1$, where g is the gain[17] $\{g = [(4\pi c)^2/\hbar\omega_2{}^3\gamma] \times (d\sigma/d\Omega)\, N\Delta$ for $\Delta\omega = 0\}$; that condition is geometry independent, as Eq. (6).

If the conditions on Δ and P_1 are met, the population in the various levels, and therefore the vibrational temperature, can be measured. To this end, one can probe simultaneously the population difference density between the ground and first vibrational levels labeled here $N\Delta_1$ instead of $N\Delta$ and that between the first and second levels ($N\Delta_2$). This can be done with a set of appropriate laser and Stokes frequencies. Sufficient anharmonicity in the vibration is needed for clear separation of the corresponding Stokes Q-branches. Note that the method is equivalent to probing the Stokes band series near the first two maxima of its sawtooth structure, as discussed in Ref. 4.

Temperature T and number density N are then uniquely determined from the set of relations

$$N\Delta_1 = N(1-e^{-\hbar\omega_v/kT})/Q$$
$$N\Delta_2 = N\Delta_1 e^{-\hbar\omega_v/kT}$$

Some inaccuracy is seen in the measurement of $N\Delta_1$ and $N\Delta_2$ as it must be done on resonance. Fortunately, the various bands have similar shapes and widths.[4] Therefore, the temperature measurement which is most conveniently obtained from the ratio $N\Delta_1/N\Delta_2$ will not be strongly affected.

3. Experimental Results

3.1. Set Up

The high power radiation at frequency ω_1 can be produced by a Q-switched laser (ruby or Nd-glass). The most elegant way to produce the pulse at the appropriate frequency ω_2 is through SRS conversion of a fraction of the pump pulse at ω_1; this is done in a high pressure cell containing the same gas to be detected. However, the technique does not work for a majority of gases because of the competition of the Stimulated Brillouin Scattering (SBS) with SRS[23]: only H_2, D_2, CH_4, N_2 and CO_2 have been found capable of producing SRS with nanosecond excitation. On the contrary SBS is ruled out with picosecond pulses, so that SRS can then build up in a larger number of gases; but the radiation linewidth (1 to 10 cm^{-1}) is large compared with the Raman linewidths (1 cm^{-1} or less). The Stokes frequency ω_2 can also be produced by a tunable dye laser which is itself pumped by part of the Q-switched laser pulse; this technique was used by Reinhold and Maier for SRS gain measurements in liquid methanol.[24] However, fine spectral tuning of the dye laser and single mode operation of both Q-switched and dye lasers are required to match the narrow vibrational Raman lines in gases (at least for $\Delta\omega = 0$).

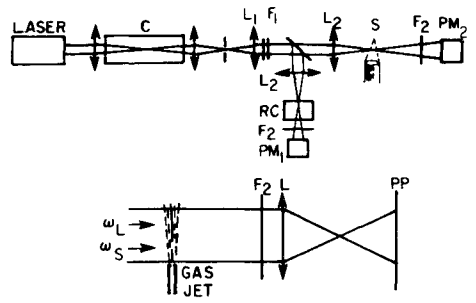

Fig. 4 Experimental arrangement (see text).

The experimental investigation presented herein was carried out with H_2; H_2 was selected because one can easily generate the Stokes sideband ω_2 by SRS. The set up is presented in Fig. 4. The single mode ruby laser is composed of a 10 cm long ruby rod, resonant reflector, cryptocyanine dye cell and 2.5-mm-diam pinhole for transverse mode selection; it delivers 40 nsec, 2 Mw pulses. The beam is focused into the SRS cell by a 20 cm focal length lens, the focal length of which was selected for nearly equal divergence of the laser and Stokes beams at the exit. The SRS cell is filled with a mixture of 80% H_2, 20% He at a total pressure of 30 atm (He is added to compensate for the pressure shift of the H_2 Raman spectrum[19]). The spectrum of the radiation emerging from the SRS cell contains a large number of sidebands corresponding to successive shifts by the $Q(1)$ vibrational transition in H_2. All but the laser and first Stokes radiations must be retained. The anti-Stokes lines are absorbed by a 6-mm-thick OG590 filter; this type of filter does not produce fluorescence in the green following multiphoton absorption of laser and Stokes light; the second Stokes component, which can combine with laser and first Stokes to produce also the first anti-Stokes component,[10] is eliminated by a 1 cm thick water cell. Spatial filtering through a 50 μm pinhole is necessary for smooth intensity profiles and excellent spatial overlap of the laser and Stokes beams. Additional color filtering after the spatial filter removes the parasitic spectral content added by the breakdown plasma at the pinhole. The beams emerging from the pinhole are either rendered parallel or refocused by lenses corrected for chromatism between 0.7 and 1 μm, depending on the application envisioned. The anti-Stokes signal P_3 from the sample (here, a flame) is separated from the laser and Stokes by several mm of Schott VG 14 glass and an interference filter centered at 5388 Å (filters F_2). Part of the pump beams can also be focused into a reference cell RC, giving the anti-Stokes reference signal P_3' and permitting normalization of P_3 (the ratio P_3/P_3' is thus independent of the fluctuations of P_1 and P_2).

In the alternate arrangement at the bottom of the figure, the signal scattered from a gas cloud or a jet is received on a high-speed photographic plate PP; lens L is not necessary, but improves the optical quality since diffraction spoils the anti-Stokes beam which would otherwise remain parallel.

3.2. Experimental Results

Coherence length

The coherence length in air was measured for the shift of H_2 (4150 cm^{-1}); we used parallel beams traversing two short cells filled with H_2. The spacing of the cells was varied, producing a sinusoidal variation of the anti-Stokes power. The period of the sine wave was 42 cm, in excellent agreement with the value calculated in Table 1.

Concentration measurements

In order to illustrate the detection capability of the equipment with the focused configuration, measurements were performed[25]

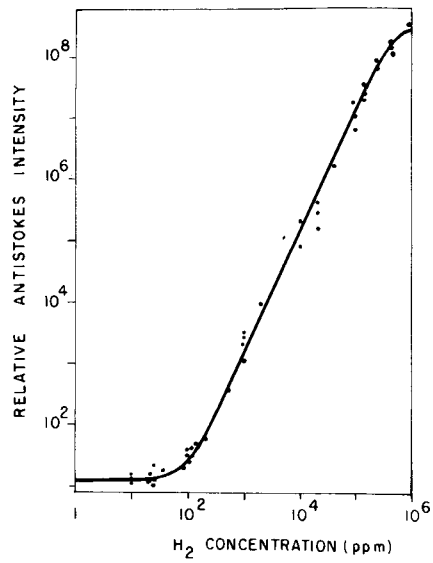

Fig. 5 Normalized anti-Stokes signal vs H_2 concentration in N_2.

on H_2 diluted in N_2, at concentrations ranging from 10 ppm to 100%. The resultant curve (Fig. 5), is a plot on a Log-Log scale of the ratio P_3/P_3' vs concentration: it exhibits a slope of 2, as expected. It departs from this behavior for both high and low concentrations.

a) For high concentrations, the combined effect of line shift and line broadening by growing concentrations of N_2 causes the observed curvature. This effect was investigated more carefully, and in particular, we found that the exciting Stokes line used for the measurements of Fig. 5 was upshifted by 2×10^{-2} cm^{-1} from the pure H_2 line. We also verified that the addition of N_2 resulted in an upshift of $+1.0\times10^{-2}$ cm^{-1} for the line, while the linewidth increased from a value of 2×10^{-2} cm^{-1} for pure H_2 (which is in agreement with the results of Lallemand and coworkers[19]) to a maximum of about 8×10^{-2} cm^{-1} for a 10:1 dilution in N_2. These results were obtained by simply scanning the line profiles by temperature tuning the SRS Stokes line (from 15° to 150°C, an almost linear frequency sweep of -6×10^{-2} cm^{-1} could be obtained).

These findings illustrate the interest of off-resonance excitation for concentration measurements as discussed in Sec. 2.3: the curvature then vanishes.

b) For low concentrations, the background contribution from the real electronic polarizability of N_2 ($\chi^{NR} \simeq 4\times10^{-18}$ esu)[13,14] gives a constant signal below 10 ppm.

This calibration curve was subsequently used to map H_2 number density profiles in a flame of natural gas premixed with

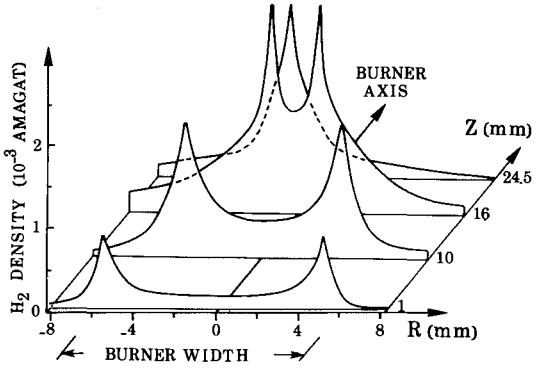

Fig. 6 H_2 distribution in a horizontal gas flame. R is the distance from the burner axis z the distance along the axis; coordinate R is vertical pointing downward.

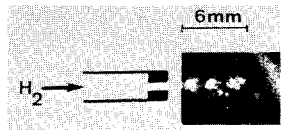

Fig. 7 Image of a supersonic H_2 jet recorded in anti-Stokes light. The streak on the upper right corner was caused by stray light.

air. The gas contained 75% methane and 25% ethane by volume, with traces of other gases (including H_2). The flame was horizontal, which explains the asymmetry in the H_2 distribution (Fig. 6). The temperature at the tip of the flame was in the vicinity of 1500°K. Scans vs radial position R were made at various distances z from the burner; the experimental points represent averages over 5 to 10 shots. No attempts were made to correct for the influence of the temperature and of the other gaseous constituents on the line shift and broadening; the experimental uncertainty associated with the latter effect can be removed, as mentioned previously, by detuning the exciting Stokes line a few linewidths. We made such measurements off resonance on our flame but failed to detect any appreciable change in distribution. This was because of the large fluctuations from shot to shot (2 ± 1) which result from the instability of the combustion. The influence of the temperature on rotational and vibrational population has not been accounted for either. The $v=0$, $J=1$ rotational level population drops by a factor of 3 from 300°K to 1500°K, while the $v=1$ population remains insignificant.

Flow visualization

With the parallel configuration of the bottom of Fig. 4 and an additional 10 cm long ruby amplifier stage inserted between the laser and the SRS cell, we were able to photograph small H_2 supersonic jets through the atmosphere, with a beam cross-section of 1 cm^2. Figure 7 gives an example of the picture recorded on 3000 ASA Polaroid film. The nozzle has a 0.8 mm internal diameter. The shock pattern in the stream can be distinguished. The N^2 dependence of the anti-Stokes intensity and the nonlinear response of the film and successive reproductions are responsible for the high contrast.

Using the high power single mode systems presently available, beam cross sections up to 10 cm in diameter can be photographed with the same sensitivity. This is of great interest for the study of combustions, explosions, and flow mixing.

4. Discussion

A new technique for gas concentration measurements has been developed and tested successfully on H_2 gas. Its detectivity (10–100 ppm) is adequate for a number of problems in aerodynamics; only moderate powers (100 kw) are needed; in addition, a capability exists for vibration temperature measurements with a more extensive range ($\simeq\hbar\omega_v/10k$ and up) than in spontaneous Raman scattering.[4]

The method applies readily to all molecular gases besides H_2 by use of tunable lasers. A set-up using a ruby laser and a dye laser is presently working in our lab and the combustion products of kerosene droplets are being studied. Measuring vibration temperatures will also tell us about the distribution of reaction energy among vibrational and translational degrees of freedom.

A possibility also exists for the remote detection of pollutants, in spite of two experimental drawbacks. First, the instrument is double ended. This reflects the need to match the wave vectors, a constraint which does not exist in SRS (where the Stokes wave

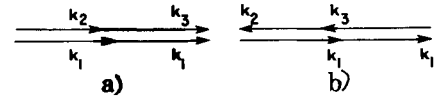

Fig. 8 Wave vector matching in CRAS: a) forward scattering; b) backward scattering.

can be generated in any direction[12]). Assuming negligible dispersion in the medium and a collinear arrangement, two configurations are possible for the k-vectors (Fig. 8). Figure 8a corresponds to our scheme, Fig. 8b to one in which both Stokes and anti-Stokes waves travel in the backward direction; in that case the detector is at close range, but the Stokes source must be remotely located, and pulse timing and beam overlap problems become severe.

Second, the detectivity is limited and should be improved by 2 or 3 orders of magnitude for practical purposes. To this end, resonant enhancement by tuning ω_1 to a discrete or a continuum absorption state would yield the same gains in detectivity as resonance excitation does in spontaneous Raman scattering,[26] with little trouble anticipated from fluorescence and quenching. Therefore, ultimate detectivities as low as 10^{-1} to 10^{-4} ppm should be achieved.

References

[1] Widhopf, G. F. and Lederman, S., "Specie Concentration Measurements Utilizing Raman Scattering of a Laser Beam," *AIAA Journal*, Vol. 9, No. 2, Feb. 1971, pp. 309–316.

[2] Hartley, D. L., "Transient Gas Concentration Measurements Utilizing Laser Raman Spectroscopy," *AIAA Journal*, Vol. 10, No. 5, May 1972, pp. 687–689.

[3] Kellam, J. M. and Glick, M. M., "Gas Density Measurements in a Jet Using Raman Scattering," *AIAA Journal*, Vol. 10, No. 10, Oct. 1972, pp. 1389–1391.

[4] Lapp, M., Penney, C. M., and Goldman, L. M., "Vibrational Raman Scattering Temperature Measurements," *Optics Communications*, Vol. 9, No. 2, Oct. 1973, pp. 195–200.

[5] Leonard, D. A., "Point Measurement of Density by Laser Raman Scattering," RN 913, June 1972, AVCO-Everett Research Lab., Everett, Mass.

[6] Mérian, M., "Application de l'Effet Raman à la Visualisation d'Ecoulements Gazeux," *La Recherche Aérospatiale*, No. 1972-2, March–April 1972, pp. 85–89.

[7] Kobayasi, T. and Inaba, H., "Spectroscopic Detection of SO_2 and CO_2 Molecules in Polluted Atmosphere by Laser-Raman Radar Technique," *Applied Physics Letters*, Vol. 17, No. 4, Aug. 1970, pp. 139–141.

[8] Hirschfeld, T., Schildkraut, E. R., Tannenbaum, H., and Tannenbaum, D., "Remote Spectroscopic Analysis of ppm-Level Air Pollutants by Raman Spectroscopy," *Applied Physics Letters*, Vol. 22, No. 1, Jan. 1973, pp. 38–40.

[9] Chang, R. K. and Fouche, D. G., "Gains in Detecting Pollution," *Laser Focus*, Vol. 8, No. 12, Dec. 1972, pp. 43–45.

[10] Maker, P. D. and Terhune, R. W., "Study of Optical Effects Due to an Induced Polarization Third Order in the Electric Field Strength," *Physical Review*, Vol. 137, No. 3A, Feb. 1965, pp. A 801–818.

[11] Lukasik, J. and Ducuing, J., "Anharmonic Coherent Raman Scattering in H_2," *Physical Review Letters*, Vol. 28, No. 18, May 1972, pp. 1155–1158.

[12] Bloembergen, N., *Nonlinear Optics*, W. A. Benjamin, New York, 1965.

[13] Rado, W. G., "The Nonlinear Third Order Dielectric Susceptibility Coefficients of Gases and Optical Third Harmonic Generation," *Applied Physics Letters*, Vol. 11, No. 4, Aug. 1967, pp. 123–125.

[14] Hauchecorne, G., Kerhervé, F., and Mayer, G., "Mesure des Interactions entre Ondes Lumineuses dans Diverses Substances," *Journal de Physique*, Vol. 32, No. 1, Jan. 1971, pp. 47–62.

[15] De Martini, F., Giuliani, G. P., and Santamato, E., "Line Profile of the $Q_{01}(1)$ Vibrational Resonance in H_2 in the zone of Dicke Narrowing," *Optics Communications*, Vol. 5, No. 2, May 1972, pp. 126–130.

[16] Yariv, A., *Quantum Electronics*, Wiley, New York, 1967.

[17] Shen, R. Y. and Bloembergen, N., "Theory of Stimulated Brillouin and Raman Scattering," *Physical Review*, Vol. 137, No. 6A, March 1965, pp. 1787–1805.

Maier, M., Kaiser, W., and Giordmaine, J. A., "Backward Stimulated Raman Scattering," *Physical Review*, Vol. 177, No. 2, Jan. 1969, pp. 580–599.

[18] Allin, E. J., May, A. D., Stoicheff, B. P., Stryland, J. C., and Welsh, H. L., "Spectroscopy Research at the McLennan Physical Laboratories of the University of Toronto," *Applied Optics*, Vol. 6, No. 10, Oct. 1967, pp. 1597–1608.

[19] Lallemand, P. and Simova, P., "Stimulated Raman Spectroscopy in Hydrogen Gas,' *Journal of Molecular Spectroscopy*, Vol. 26, 1968, pp. 262–276.

[20] Ward, J. F. and New, G. H. C., "Optical Third Harmonic Generation in Gases by a Focused Laser Beam," *Physical Review*, Vol. 185, No. 1, Sept. 1969, pp. 57–71.

[21] Régnier, P. R., "Application de la Diffusion Anti-Stokes Cohérente à la Mesure des Concentrations Gazeuses et à la Visualisation des Ecoulements," thesis, Paris 11, Nov. 1973.

[22] Audibert, M., Joffrin, C., and Ducuing, J., "Vibrational Relaxation in Hydrogen-Rare Gases Mixtures," *Chemical Physics Letters*, Vol. 19, No. 1, March 1973, pp. 26–28.

[23] SBS has a lower threshold than SRS, but its response time is generally longer. See Carman, R. L. and Mack, M. E., "Experimental Investigation of Transient Stimulated Raman Scattering in a Linearly Dispersionless Medium," *Physical Review A*, Vol. 5, No. 1, Jan. 1972, pp. 341–348, and the references therein.

[24] Reinhold, I. and Maier, M., "Gain Measurements of Stimulated Raman Scattering Using a Tunable Dye Laser," *Optics Communications*, Vol. 5, No. 1, April 1972, pp. 31–34.

[25] Régnier, P. R. and Taran, J.-P. E., "On the Possibility of Measuring Gas Concentrations by Stimulated Anti-Stokes Scattering," *Applied Physics Letters*, Vol. 23, No. 5, Sept. 1973, pp. 240–242.

[26] Fouche, D. G. and Chang, R. K., "Observation of Resonance Raman Scattering below the Dissociation Limit in I_2 Vapor," *Physical Review Letters*, Vol. 29, No. 9, Aug. 1972, pp. 536–539.